Nano Research

Open Access

Research Article

Platelet-derived extracellular vesicles for endometrial regeneration towards efficient live birth

Dongxiao Li[1], Yanhong Yang[1], Bo Tian[3], Chenmeng Zhou[2], Shuting Gu[1], Wenju Chang[3], Bingbing Wu[2], Dantong Dong[1], Fang Xu[2], Ziyang Yu[1], Ling Zhou[1], Chao Wang[2] ✉, and Hong Zhang[1] ✉

[1] *Department of Obstetrics and Gynecology, The Second Affiliated Hospital of Soochow University, Suzhou 215004, China*
[2] *Institute of Functional Nano & Soft Materials (FUNSOM), Soochow University, Suzhou 215123, China*
[3] *Department of Orthopedics, The Second Affiliated Hospital of Soochow University, Suzhou 215004, China*

Cite this article: *Nano Research*, **2025**, *18*, 94907176. https://doi.org/10.26599/NR.2025.94907176

ABSTRACT: Uterine infertility is a major global issue causing substantial physical and psychological hardship for individuals struggling to conceive, while endometrium injury is one of the crucial factors causing infertility. Here, we demonstrate that platelet-derived extracellular vesicles (PEVs) have excellent regenerative ability in treating endometrial injuries, facilitating endometrium regeneration and resulting in a highly efficient live birth rate in the endometrium-injured murine model. We further investigated the underlying mechanisms by which PEVs affect the endometrium, showing their ability to promote neovascularization and suppress fibrosis. More importantly, the regenerative endometrium is more receptive to embrace the embryo, which can sustain the normal pregnancy. Our finding serves as a foundational basis for advancing the clinical translation of platelet-rich plasma (PRP) and PEVs therapies for endometrial regeneration.

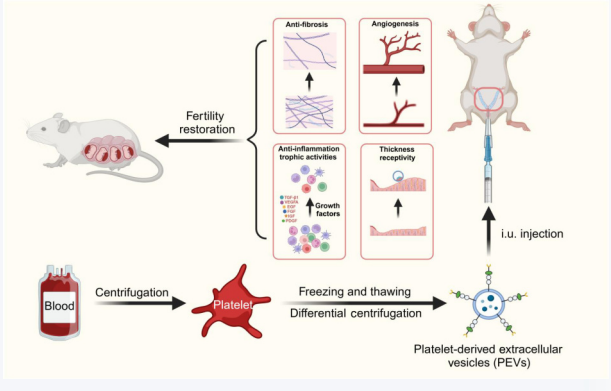

KEYWORDS: endometrium regeneration, fertility restoration, platelet-derived extracellular vesicles, platelet-rich plasma

1 Introduction

Infertility is a worldwide challenge that almost 17.5% (one out of six) of the childbearing-aged population suffers from [1, 2], due to the associated emotional distress and societal pressures surrounding childbearing, thereby those patients urgently need affordable and high-quality reproductive health services. Among all the factors of infertility, endometrial injury is an increasingly common one, which is also the bottleneck problem of assisted reproductive technology (ART) [3, 4]. Intrauterine adhesion (IUA) is partial or complete occlusion of the uterine cavity due to endometrium injury, often accompanied with severe clinical problems, such as hypomenorrhea, amenorrhea and infertility [5, 6]. It is reported that an appropriate endometrial thickness is essential for both the beginning and ongoing of pregnancy [7–9]. However, several factors can result in thinness of the endometrium, including endocrine factors, repeated improper curettage, medical interventions, or infections that damage the endometrial basal layer. Currently, the standard clinical strategies for injured endometrium are estrogen, cytokines, sildenafil citrate, low-dose aspirin, surgery, and even stem-cell therapy [10]. Among them, platelet-rich plasma (PRP), an autologous concentrated plasma product with platelets (PLTs) above baseline, has shown promise as a regenerative therapy to promote healing and regeneration of the endometrium [11–13]. However, the underlying molecular mechanisms by which PRP affects the endometrium are still not fully understood [14]. The lack of a clear mechanism makes it challenging to optimize the therapy, especially in complex cases. Meanwhile, as an emerging treatment for endometrial regeneration, PRP has controversial defects, like costly, absence of a standardized protocol for preparation, complicated composition individually, etc. Variations in platelet concentration and the presence of other blood components can lead to inconsistent results and patient response variability. Moreover, the most abundant PLTs of PRP are easily affected by various conditions (such as temperature, shake, and pollution) during storage and transportation, resulting in PLTs activation and an inflammatory response [15, 16]. As a result, the consensus on

Received: September 30, 2024; **Revised:** November 21, 2024
Accepted: December 5, 2024

✉Address correspondence to Chao Wang, cwang@suda.edu.cn; Hong Zhang, szzhanghong126@126.com

PRP bio-formulations and well-documented clinical evidence are nonexistent at present [17].

Platelet-derived extracellular vesicles (PEVs) are a group of bilayer vesicles that not only retain the characteristics of platelets but also contain the advantages of nanosize effect [18–20]. Due to the nanosize, they are more effective to carry and deliver bioactive molecules, facilitate communication with targeted cells, enhance signal transduction and immunomodulation compared with platelet [21]. More importantly, PEVs offer several advantages over whole platelets for storage and transportation, particularly in terms of stability, flexibility, and reduced immunogenicity [22–24]. Here, we find that PEVs are critical components contributing to the regenerative potential of PRP in treating endometrium injuries [19]. By intrauterine administration, PEVs were retained in the uterus for a relatively long time, exhibiting an excellent ability for endometrium regeneration and achieve a highly efficient live birth rate versus controls. We further investigated the underlying mechanisms by which PEVs affect the endometrium, showing their ability to promote angiogenesis, anti-fibrosis and suppress the inflammation. These findings serve as a foundational basis for advancing the clinical translation of PRP and PEVs therapies for endometrial regeneration.

2 Experimental

2.1 Animal

Female Kunming (KM) mice (6–8 weeks old) weighing about 25–28 g were purchased from Beijing Vital River Laboratory Animal Technology Co., Ltd. The animals were housed in a specific pathogen free (SPF) barrier at stationary temperature (25 ± 2 °C) and humidity (45%–55%), with a 12 h-day/night cycle and free access to food and water. We performed all mice experiments in accordance with the ethics approved by our university ethics committee (approval number: SUDA20231012A02). Experimental group sizes were approved by the regulatory authorities for animal welfare after being defined to balance statistical power, feasibility, and ethical aspects. The mice were acclimatized for one week and vaginal smears were obtained daily at 08:00–10:00 a.m. to determine the stage of the estrous cycle. In total, female mice with regular oestrus cycles were selected for the subsequent experiments.

2.2 Endometrial injury model construction and treatment

The selected mice were randomly divided into three groups. Sham group: only laparotomy. UNTX group: mice with uterine injury surgery without any treatment. PEVs-treated group: mice with uterine injury surgery treated with intrauterine PEVs (50 μg/day for each uterine horn).

The mice model of endometrial damage was established as previously described. 1% pentobarbital sodium was applied to anesthetize the mice through intraperitoneal injection at a dose of 10 μL/g. A small vertical incision was made into the inferior abdomen to expose the uterus, and then 95% ethanol (EtOH) was injected into the uterus, clamped by microhemostatic clamps, for one minute using a 31-gauge insulin syringe and rinsed with 0.9% saline repeatedly. After the abdominal cavity was washed with 0.9% saline, it was stitched using 4-0 absorbable sutures.

2.3 Preparation and characterization of PEVs

Mice platelets were separated according to the protocol reported previously. Briefly, whole blood was collected from the sinus of KM mice in a tube containing 200 μL acid-citrate dextrose (ACD) anticoagulant (KWS, China) and 1 mM prostaglandin E1 (PGE1) (HY-B0131, MCE), then centrifuged at 0.1 G for 15 min to remove red blood cells. Repeat 0.1 G for 3 min is needed when the red blood cell is still visible. The supernatant was collected and centrifuged at 0.8 G for 20 min to obtain the platelets. Then, 500 μL sterile Dulbecco's phosphate buffered saline (DPBS) (P1006, Solarbio) was used to re-suspend and centrifuge again to obtain purified platelets. Subsequently, repeated freezing (−80 °C, 24 h) and thawing (37 °C, 40 min) process three times and centrifugation (0.3 G, 10 min; 1.5 G, 15 min, 3.2 G, 20 min; 100,000 rpm, 2 h) to concentrate the PEVs into granules. The morphology of PEVs was detected by transmission electron microscopy (TEM). Protein expression of PEVs was determined by sodium dodecyl sulfate-polyacrylamide gel electrophoresis (SDS-PAGE), western blot, and mass spectrometry. The particle size and changes over time were measured by dynamic light scattering (DLS).

2.4 TEM

20 μL fresh PEVs solution was added to a 300 mesh copper mesh (BZ11023a, EMCN) placed on filter papers and incubated for 5 min. Subsequently, 1% phosphotungstic acid solution was applied for negative staining and incubated for 5 min, washed with ddH_2O to dry for TEM. The images were acquired using an FEI TF20 transmission electron microscope at 200 kV.

2.5 DLS

The particle size and zeta potential of PEVs were determined by DLS: The volume of the PEVs sample was increased to 1 mL by DPBS and loaded into a quartz cuvette. The size distribution and zeta potential of PEVs were measured by dynamic light scattering at 25 °C and analyzed using FLEX software. We also tested the stability of the PEVs by measuring the particle size changes for 7 consecutive days by using DLS.

2.6 SDS-PAGE

The PEVs were dispersed in a loading buffer (WB2001, NCM biotech). The samples were then added to a 10% gel (PG122, Epizyme), and the proteins were separated in a running buffer (G2018-15, Servicebio) using an electrophoresis system (Bio-rad). Finally, the protein bands were stained by Coomassie Blue (PS111, Epizyme).

2.7 Western blot

Samples were lysed on ice using RIPA buffer (PC101, Epizyme) supplemented with phosphatase and protease inhibitors cocktail (P1045, Beyotime) to resolve total proteins with proteins protected. Proteins in samples were normalized according to bicinchoninic acid assay (BCA) results, separated by SDS-PAGE (PG122, PG123, Epizyme), and then transferred to polyvinylidene fluoride (PVDF) membranes (0.22 μm, ISEQ00010, Sigma Aldrich). The membranes were blocked with non-fat milk for 2 h at room temperature (RT) and then incubated at 4 °C overnight with primary antibodies at proper dilution (1:1000). Secondary antibodies at appropriate dilution (1:5000) were incubated with membranes for 1 h after Tris buffered saline with Tween (TBST, G0001, Servicebio). Enhanced chemiluminescence (ECL) (P10060, NCM biotech) reagent was utilized for band visualization, and ImageJ software was used for

image quantification. Antibodies used for immunoblotting were shown as following: CD9 Rabbit PolyAb (20597-1-AP, Proteintech), CD63 Rabbit PolyAb (Abs132700, Absin), CD41 Rabbit PolyAb (TD7456S, Abmart), β-actin Rabbit mAb (4970T, CST), GAPDH Rabbit PolyAb (10494-A-AP, Proteintech), P-selectin/CD62P Mouse McAb (60322-1-Ig, Proteintech), Sodium Potassium ATPase Rabbit pAb (ab58475, Abcam). The secondary antibodies anti-mouse IgG HRP-linked (SA00001-1), anti-rabbit IgG HRP-linked (SA00001-2), and anti-rat IgG HRP-linked (SA00001-15) were purchased from Proteintech.

2.8 Mouse growth factor assay

The assay was performed following the manufacturer's protocol (AssayGenie, SARB0088). Briefly, after adjusting the membranes into the incubation chamber, the membranes were blocked by adding 2 mL blocking buffer to each incubation well for 30 min at room temperature. 100 μg proteins were incubated with the antibody membrane overnight at 4 °C. After that period, samples were discarded and the membranes were washed 3 times for 5 min with 2 mL wash buffer I and twice for 5 min with 2 mL wash buffer II. Then, the membranes were incubated with a biotinylated antibody cocktail overnight at 4 °C. Again, the membranes were washed five times as previously and incubated with horseradish peroxidase (HRP)-streptavidin at 4 °C overnight. Chemiluminescence was used to detect signals of the growth factors spotted on the nitrocellulose membrane.

2.9 Cell lines

RAW264.7 cells (mouse monocyte macrophages), DC2.4 cells, and Ishikawa cells were originally purchased from the American Type Culture Collection (ATCC). hESCs cells (human endometrial stromal cells) were donated by Prof. Haibin Wang from Xiamen University. In detail, RAW264.7 cells were cultured in L-DMEM medium containing 10% fetal bovine serum (FBS, Gibco), and 1% penicillin-streptomycin (C100C5, NCM biotech). DC2.4 cells were maintained in RPMI1640 medium with 10% FBS and 1% penicillin-streptomycin. Ishikawa cells were cultured in DMEM/F12 medium supplemented with 10% FBS and 1% penicillin-streptomycin. hESCs cells were cultured in phenol red-free DMEM/F-12 (11039-021, Gibco) containing 10% (v/v) charcoal-stripped fetal bovine serum (CS-FBS, C3830-0500, Viva Cell), 1 mM sodium pyruvate (P6033, Macklin), supplemented with 1.5 g/L sodium bicarbonate (S6014, Sigma), 1% penicillin-streptomycin, 1% Insulin-Transferrin-Selenium (ITS, 41400-045, Gibco), and 500 ng/mL puromycin (HY-B1743A, MCE).

2.10 Cell proliferation and viability

The biocompatibility of PEVs on several cell strains was determined with 3-(4,5-dimethylthiazol-2yl)-2,5-diphenyltetrazolium bromide (MTT) assay. RAW264.7, DC2.4, hESCs, and Ishikawa cells were seeded in 96-well plates and proliferated in the corresponding medium at a density of 5×10^3 cells/well for 24 h. Then, the medium containing different concentrations of PEVs was changed, and cells were cultured for another 24 h. Then, the medium containing MTT (5 mg/mL) was replaced in each well and incubated for an additional 2 h at 37 °C. Then, the crystals were dissolved in dimethyl sulfoxide (DMSO) and detected at 490 nm (OD490) by a Bio-Tek microplate reader (BioTek, Winooski, VT, USA). Compared with the absorbance values of untreated controls, cell viability was calculated.

2.11 Retention rate of PEVs (*in vivo* imaging system (IVIS))

Mice were first anesthetized with isoflurane mixed with oxygen, followed by intrauterine administration of DiR-labeled PEVs (DiR, HY-D1048, MCE), with four mice in each group. Then, sutures were used to ligature the cervix for 2 h, aiming to retain PEVs in the mice uterus for a period of time which can imitate the real clinical scenario that patients would keep in the lithotomy position for a while after intrauterine perfusion. After 24 h, the IVIS Spectral Imaging System (PerkinElmer Ltd.) was used to monitor the retention of PEVs in the uterus. The major organs were also collected for *in vitro* imaging. Fluorescence intensity was quantified as total radiance ([p/s]/[μW/cm^2]) with IVIS Living Image 4.2. The expression level of DiR in the uterus tissue was observed by confocal imaging.

2.12 Immunofluorescence (IF)

For immunofluorescence, cells or tissue sections were fixed in 4% paraformaldehyde (PFA) for 15 min, blocked with 10% FBS for 120 min at RT and incubated with primary antibodies at 4 °C overnight and secondary antibodies at RT for 1 h, then, stained with DAPI (G1012, Servicebio). Antibodies used for immunofluorescence were shown as follows: Phalloidin-488 (YP0059S, UElandy), PSGL-1 Rabbit mAb (1:1000, A23373, Abclonal). The secondary antibodies goat anti-rabbit Alexa Fluor 594 (A11012), with a dilution at 1:200, was purchased from Invitrogen.

2.13 Flow cytometry (FCM)

The mice uteri were collected after 24 h of intrauterine perfusion and prepared as single-cell suspensions for flow cytometry analysis. Mice uterine tissues were minced with scissors and digested at 37 °C for 40 min with type IV collagenase (1.0 mg/mL, Sigma, C5138) prepared in RPMI 1640. The digested tissues were then ground and passed through a 70 μm strainer to obtain a single-cell suspension. And for cells, they can be stained after washing with 3% bovine serum albumin (BSA) at 1000 rpm, 4 min, 4 °C. The relative fluorescence intensities of DiR in dendritic cells (DCs) (PECY7-CD45 and FITC-CD11c), granulocytes (PECY7-CD45 and APC-GR1), macrophages (PECY7-CD45 and APC-F4/80), T cells (PECY7-CD45 and APC-CD3), monocytes (PECY7-CD45 and APC-CD14) and non-immune cells (PECY7-CD45$^-$) were analyzed to determine the relative uptake of PEVs.

2.14 Histological analysis

After treatment, the uteri of different time points in each group were obtained, cleaned in saline to remove excess blood, fixed in 4% paraformaldehyde solution, and then embedded in paraffin. The paraffin sample was cut into 4-μm-thick slices for hematoxylin and eosin staining (H&E staining), Masson staining, and immunohistochemistry (IHC staining). Afterward, the samples were sealed with neutral resin, micrographs were captured, and the proportion of positive areas was analyzed using the ImageJ software, the thickness of endometrium was measured by Image Pro plus 6.0.

2.15 Statistical analysis

All data in the present study are expressed as mean ± standard deviation (SD). The significance of differences between two groups was calculated by a two-tailed unpaired Student's t test. In addition,

analysis of variance (ANOVA) comparisons and Bonferroni's post hoc tests were performed between more than two groups (multiple comparisons). All statistical analyses were performed using GraphPrism (v9.5). Values of $P < 0.05$ were considered significant. All intensities of fluorescence expression in the experiments were further calculated by ImageJ software. The standard symbols were presented as $^{*}P < 0.05$, $^{**}P < 0.01$, $^{***}P < 0.001$.

3 Results

3.1 Preparation and characterization of PEVs

Several studies have reported positive outcomes with PRP treatment in endometrium-damaged patients, while the underlying mechanism is still not fully understood. Here, we hypothesize that PEVs, which are critical components in PRP, contribute to the regenerative potential of PRP in treating endometrium injuries. We prepared the PEVs through freezing and thawing repeatedly as a standard protocol [18, 25, 26] (Fig. 1(a)). The purified PEVs (Fig. 1(b)) showed a spherical structure with a size of about 100 nm under the TEM (Fig. 1(c)) image and DLS analysis, compared with PLTs with a size of nearly 1 μm. The zeta potentials of PEVs are negative (Fig. 1(d)). The size of PEVs remained stable stored at low temperatures, indicating the high stability of PEVs *ex vivo* (Fig. 1(e)). Besides, Coomassie brilliant blue staining (Fig. 1(f)) and western blot were used to ensure that the obtained vesicles were derived from platelets. The membrane marker proteins (CD9, CD41, and CD63) were significantly enriched, cell adhesion-related protein (P-selectin) was retained and cytoplasmic proteins of PLTs (glyceraldehyde-3-phosphate dehydrogenase (GAPDH) and β-actin) were lower in PEVs (Fig. 1(g), and Fig. S1 in the ESM). Meanwhile, PEVs showed high biocompatibility (Fig. S2 in the ESM), and carry various bioactive molecules, including growth factors, which are essential for tissue repair, regeneration, and modulation of inflammatory responses. Multiple key growth factors (such as vascular endothelial growth factor A (VEGFA); transforming growth factor-β (TGF-β); epidermal growth factor (EGF); fibroblast growth factor (FGF); insulin-like growth factor (IGF); platelet-derived growth factor (PDGF)) were still retained in the vesicle (Fig. 1(h), and Fig. S3 in the ESM), which protect them from degradation in the extracellular environment and facilitate their targeted delivery to specific cells or tissues. These results suggest that the proteins within the PEVs could initiate tissue repair and regeneration upon reaching their target cells.

3.2 *In vivo* targeting of PEVs to injured endometrial tissue

In our previous studies, we have demonstrated that PEVs exhibited great targeting capacity to various inflammatory sites. *In vitro*, to mimic the inflammatory microenvironment, we converted RAW264.7 and hESCs to proinflammatory status by lipopolysaccharide (LPS) pre-treatment. The activated cells were then incubated with PEVs labeled with 1,1-dioctadecyl-3,3,3,3-tetramethylindotricarbocyaine iodide (DiR) for 30 min. As shown by fluorescence imaging, PEVs showed a higher affinity toward activated cells compared with the non-activated cells (Figs.

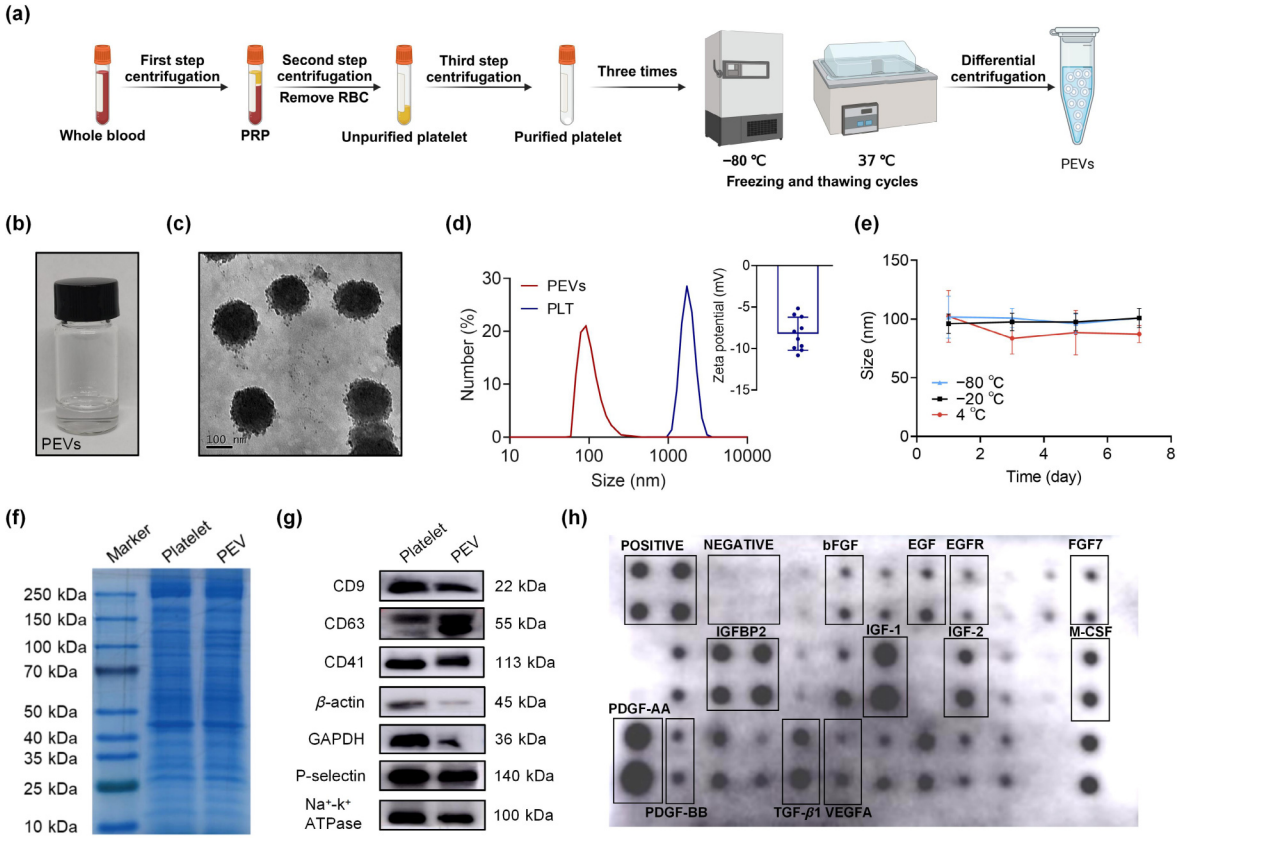

Figure 1 Characterization of the platelet-derived extracellular vesicles. (a)Scheme of preparing PEVs. (b) Photograph of PEVs resuspend in DPBS. (c) TEM image of PEVs (scale bar: 100 nm). (d) PEVs size distribution and zeta potential measured by DLS. (e) Particle size of PEVs stored for 7 days at different temperature (4, −20, −80 °C). (f) SDS-PAGE of platelet lysate and PEVs with Coomassie brilliant blue staining. (g) Western blot analysis of CD9, CD63, CD41, β-actin, GAPDH, P-selectin, and Na^{+}-K^{+} ATPase from the platelet lysate and PEVs. (h) Growth factors array of PEVs.

2(a)–2(d)). *In vivo*, we established an endometrium-damaged mice model according to the protocol (Fig. S4 in the ESM). To simulate the clinical scenario, we intrauterine perfusion of PEVs-DiR and ligated the cervix with sutures and left both ends outside the body, aiming to allow PEVs to stay in the uterine cavity of the mice for 2 h before loosening the slipknot and untied the cervix (Fig. 2(e)). The sham surgery mice were used as a control. Another 22 h later, the major organs were collected and imaged by an *ex vivo* imaging system. Interestingly, we observed much higher retentions of PEVs-DiR in the uterus of the model mice versus sham controls (Fig. 2(f)). In addition, the flow cytometry and confocal results of endometrial tissue also showed the enrichment of PEVs signals compared with the control uterus (Figs. 2(g) and 2(h)), further confirming the targeting capacity of PEVs to the injured endometrial tissue. PEVs express adhesion molecules like P-selectins (Fig. 1(g)), which facilitate their binding to the cells expressing receptors like P-selectin glycoprotein ligand-1 (PSGL-1) at the injury endometrium in mice (Fig. 2(i)). This targeting ability was associated with the specific ligands on PEVs that bind to receptors on the surface of the injured endometrial cells or the immune cells.

3.3 Efficacy of PEVs for the repair of damaged endometrium

To verify the effectiveness of PEVs to uterus recovery systematically, we constructed an endometrial injury mice model by intrauterine (i.u.) injection of 95% ethanol [27–29] (Fig. 3(a), and Figs. S4 and S5 in the ESM). In our experiment, the mice were randomly divided into three groups: Healthy (Sham) mice, Untx mice (mice with endometrial injury without treatment), and PEVs-treated mice (mice with endometrial injury treated by PEVs (i.u. 50 μg/uterine horn for consecutive three days)). In the following days, the gross views and tissue section staining of the uterus were captured and analyzed.

Compared with healthy (Sham) mice, obvious damage in the endometrium and myometrium was observed in Untx mice, leading to structural and functional impairments of uterine tissue. In contrast, the uterus progressively improved over time and almost without hydrometra or stenosis in the PEVs-treated mice (Figs. 3(b) and 3(c)). Damaged uterine tissue exhibited remarkable thinning of the endometrial layers, which were indistinguishable from the myometrium in some areas. In mice receiving PEVs, endometrial regeneration was observed, as evidenced by the presence of well-distributed cells and apparent neovascularization and endometrial thickness. In Untx mice, endometrial thickness was reduced from 150 to 70 μm, indicating the remarkable injury of endometria. Surprisingly, the thickness was recovered significantly in the PEVs-treated mice, and the structure of the uterus was nearly regenerated to normal on day 15, similar to the healthy (Sham) group (Figs. 4(a) and 4(b)). Besides, endometrial tissue was well-organized in PEVs-treated mice, with appropriate epithelial and secretory gland organization. In addition, the number of endometrial glands plays a crucial role in endometrial repair, as these glands are responsible for secreting essential factors that promote tissue regeneration, maintain endometrial integrity, and support functional recovery after injury or damage. Consistently, the trends in the number of glands closely mirrored those observed for endometrial thickness across the different treatment groups, further highlighting their

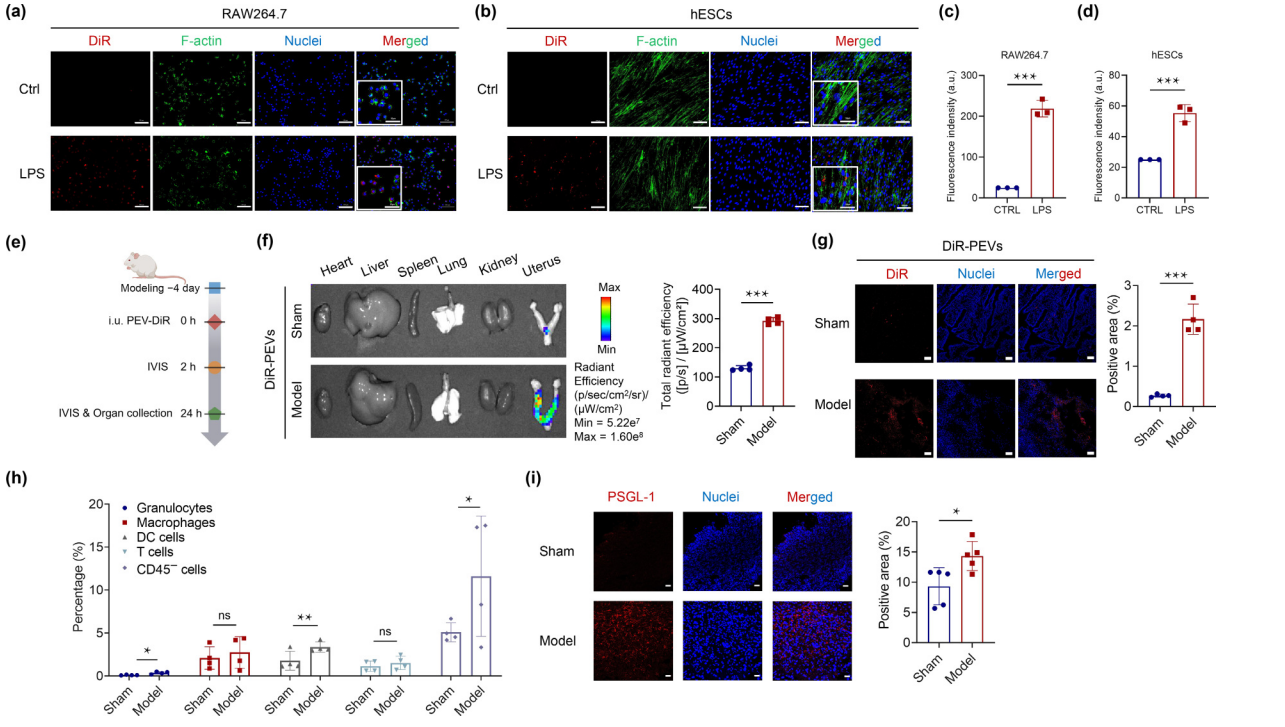

Figure 2 *In vivo* targeting property of PEVs. Confocal fluorescence imaging of DiR-labeled PEVs after incubation with activated (a) RAW264.7 and (b) hESCs, and corresponding quantitative analysis of (c) RAW264.7 and (d) hESCs. (e) Schematic diagram of the timeline of animal experiments to test the *in vivo* targeting properties of PEVs. (f) *Ex vivo* fluorescence imaging of major organs and uterus in KM mice after various treatments as indicated at 24 h and corresponding quantitative analysis. (g) Immunofluorescence of uterus tissue slices of mice after different treatments as indicated (blue: nuclei; red: PEVs) (scale bars: 50 μm) and corresponding quantitative analysis. (h) Signal of DiR among granulocytes, macrophages, DCs, T cells, and $CD45^-$ cells in the uterus after 24 h by flow cytometry analysis (4 uterus samples in each group). (i) Immunofluorescence images of PSGL-1 in murine uterus (scale bars: 20 μm) and corresponding quantitative analysis. Statistical significance was determined by Student's t-test (two-tailed). $^{***}P < 0.001$; $^{**}P < 0.01$; $^{*}P < 0.05$. The data are presented as mean ± SD.

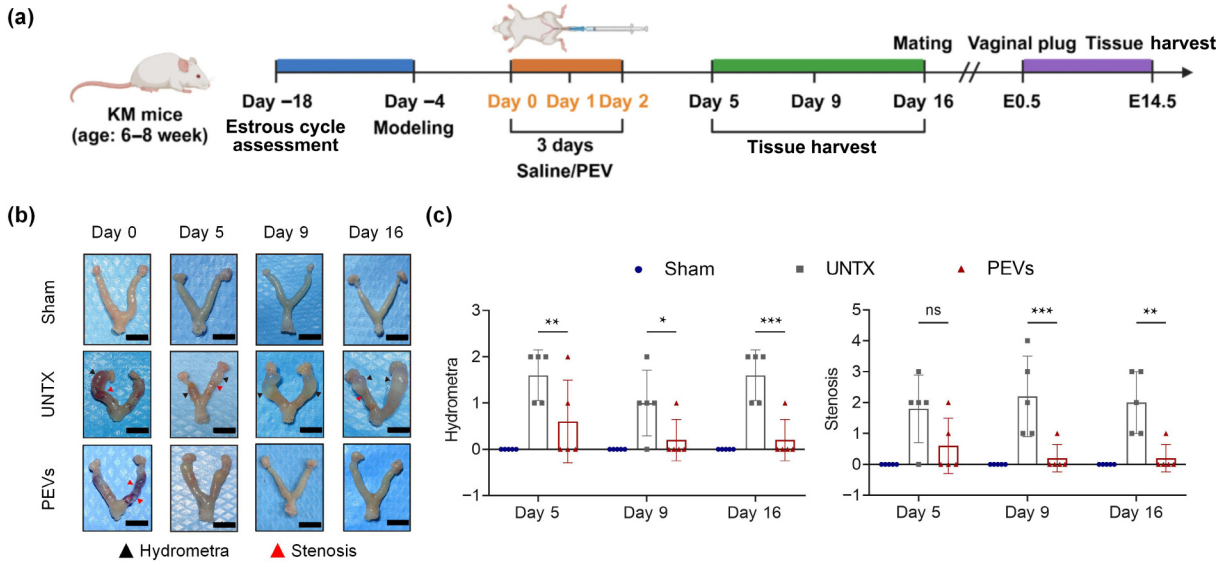

Figure 3 Efficacy of PEVs for the repair of damaged endometrium.(a) Schematic diagram of PEVs to treat damaged endometrium. (b) Gross views of the uterus after treatment at different time points (scale bars: 1 cm). (c) Quantitative analysis of hydrometra and stenosis in different treatment groups at different time points. Statistical significance was determined by Student's t-test (two-tailed) and one-way analysis of variance (ANOVA) with the Bonferroni post hoc test. ***$P < 0.001$; **$P < 0.01$; *$P < 0.05$. The data are presented as mean ± SD.

interconnected roles in endometrial repair. Specifically, there was an average of 46 glands in mice receiving PEVs, which was 76% of that observed in the healthy (Sham) mice and 8 times of that observed in the Untx mice (Fig. 4(c)), reaffirming the ability of PEVs to promote tissue regeneration.

We further assessed the collagen deposition via Masson trichrome staining. The data demonstrated an effective anti-fibrosis and inflammatory suppression ability of PEVs, thereby driving well-developed vascular and glandular proliferation in the damaged endometrium of mice (Figs. 4(d) and 4(e)). Given that endometrial regeneration is dependent upon angiogenesis to deliver appropriate oxygen and nutrient supplies to tissue regeneration, we next sought to determine whether the PEVs can promote angiogenesis *in vivo*. To that end, endometrial tissue was stained for the endothelial cell marker CD31, revealing that endometrial tissue samples from the PEVs treated mice exhibited significantly increased CD31 staining relative to the Untx group (Figs. 4(f) and 4(g)).

3.4 Conceptions after PEVs intervention

Infertility and uterine injury are closely interconnected, as the endometrium is responsible for the implantation of the embryo, supporting fetal development, and maintaining a pregnancy to term. Any severe injury or damage to the endometrium can significantly impair these processes, potentially leading to infertility, pregnancy complications, or poor reproductive outcomes.

Conception is considered the gold standard for assessing the recovery of endometrium function. To assess the healing function of PEVs in mice with severe endometrial injury, we conducted a comprehensive fertility analysis involving embryo implantation and placental development. On the 16th day after modeling, all female mice were mated with healthy male mice at a ratio of 2:1, and the success of mating was determined by vaginal plugs, which were designated as E0.5. At E14.5, the mice were euthanized and the fetuses as well as the placentas were collected for further analysis. As expected, no fetuses and placentas were observed in Untx mice, indicating that injury or damage of the uterus leads to infertility. Strikingly, the litter size of the mice receiving PEVs was significantly improved (Figs. 5(a)–5(c)). The average weight of embryos (Fig. 5(d)) and placentas (Fig. 5(e)) from mice receiving PEVs was comparable to that of the healthy (Sham) controls, suggesting that the repaired uteri could sustain normal fetal development (Fig. 5(f)).

4 Conclusions

In conclusion, we first applied and evaluated the therapeutic effects of PEVs on the injured endometrium, and PEVs could be an optimal alternative to PRP due to their advantages, including low immunogenicity, stability, and nanosize effect. In addition, PEVs can increase the thickness of endometrium and implantation rate in murine model through promoting neovascularization and suppressing inflammation. Owing to the ease of preparation, low cost, and clear mechanism, PEVs would be a promising therapeutic avenue for human beings with thin endometrium.

Electronic Supplementary Material: Supplementary material (antibodies applied in study, uncropped blots, cell viability analyses, procedure of modeling, etc.) is available in the online version of this article at https://doi.org/10.26599/NR.2025.94907176.

Data availability

All data needed to support the conclusions in the paper are presented in the manuscript and/or the Electronic Supplementary Material. Additional data related to this paper may be requested from the corresponding author upon request.

Acknowledgements

This work was partly supported by the National Key R&D Program of China (No. 2022YFB3808100). This work was supported by National Natural Science Foundation of China (Nos. 81873835 and 82071726), the Suzhou Science and Technology Plan (No. SKY2022005), the Gusu Talent Project of Suzhou (No.

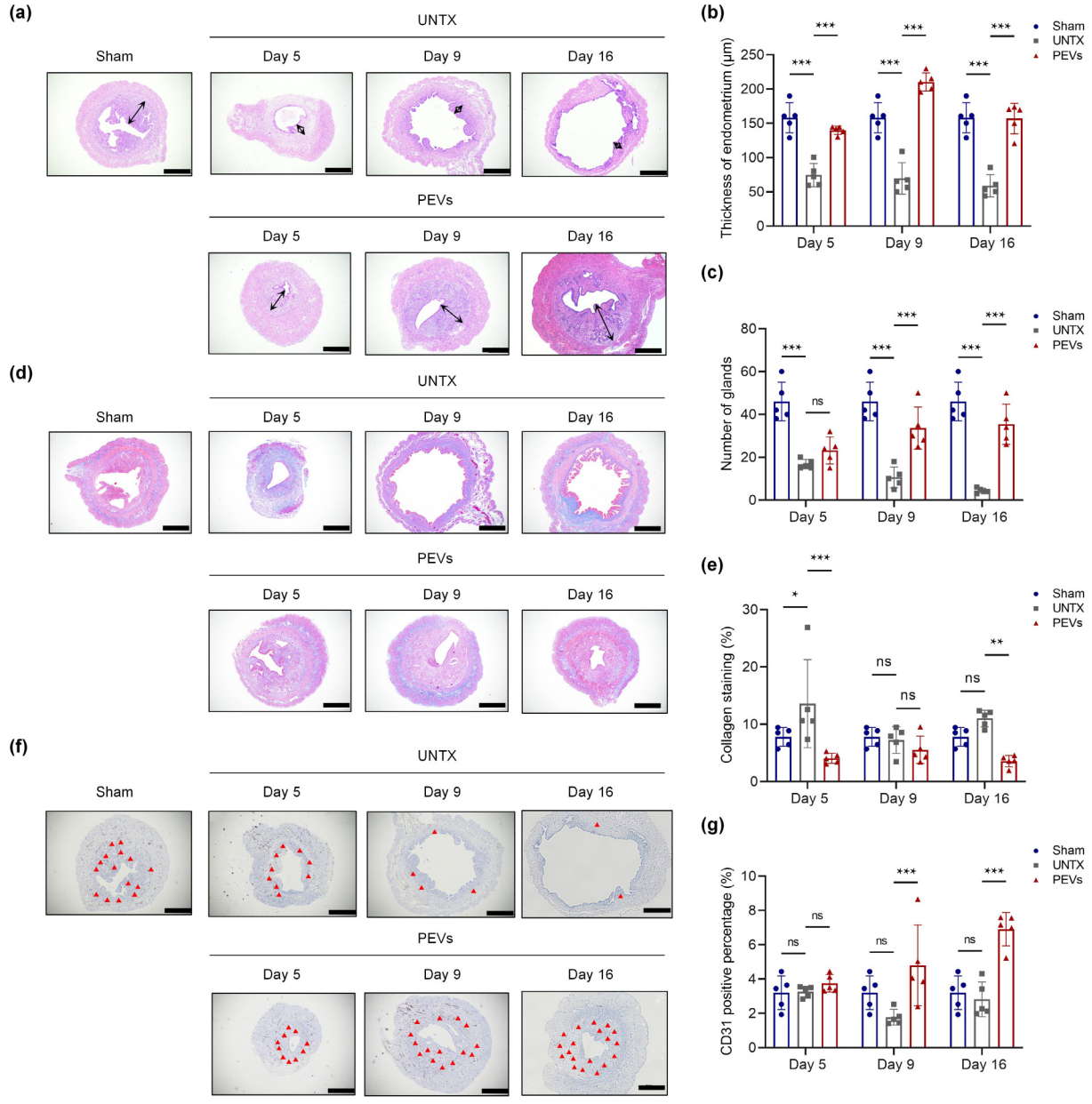

Figure 4 The treatment assessment of mouse with different interventions at different points. (a) H&E staining of the cross-section of uterus after treatment at different time points (scale basr: 500 μm), and corresponding quantitative analysis of (b) thickness of endometrium and (c) number of glands. (d) Masson staining of the cross-section of uterus after treatment at different time points (scale bars: 500 μm) and (e) corresponding quantitative analysis. (f) Immunohistochemical staining of CD31 of the cross-section of uterus after treatment at different time points (scale bars: 500 μm) and (g) corresponding quantitative analysis. Statistical significance was determined by Student's t-test (two-tailed) and one-way analysis of variance (ANOVA) with the Bonferroni post hoc test. ***$P < 0.001$; **$P < 0.01$; *$P < 0.05$. The data are presented as mean ± SD.

GSWS2020011), the Science and Technology Project of Suzhou (No. SKY2023138) and the research fund of the Second Affiliated Hospital of Soochow University (No. SDFEYGZ2319).

Declaration of competing interest

All the contributing authors report no conflict of interests in this work.

Author contribution statement

H. Z., C. W., and D. X. L. designed the experiments. D. X. L. performed main experiments, analyzed data and wrote the draft of the manuscript. Y. H. Y., B. T., C. M. Z., S. T. G., W. J. C., Z. Y. Y., and L. Z. supported experiments and data analysis. B. B. W., D. T. D., and F. X. gave some suggestions and reviewed writing. All authors read and approved the final manuscript.

Informed consent

Not applicable.

Ethics statement

The animal experiments were carried out following the guidelines of Soochow University Institutional Committee for the Care and

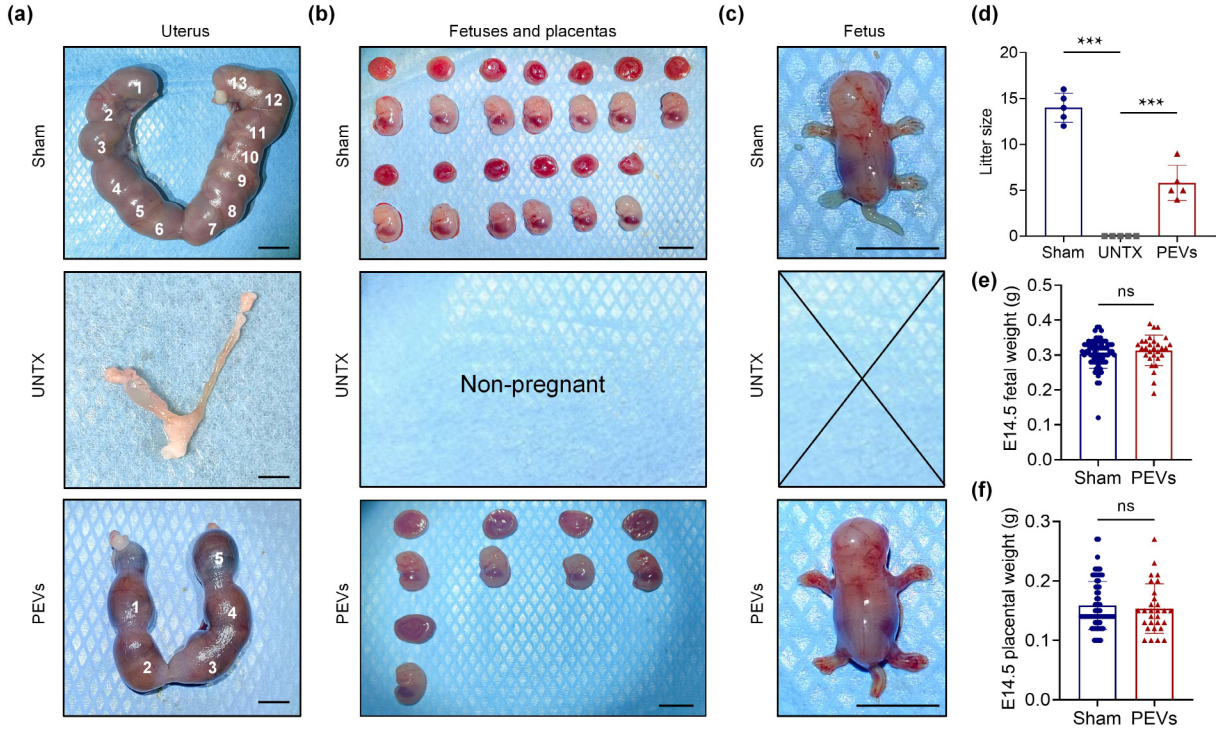

Figure 5 Live births in different groups and the assessments of fetus and placenta. Live birth outcomes represented by (a) uterine morphology, (b) fetuses and placentas, and (c) fetal morphology across different treatment groups (n = 5, scale bars: 1 cm). (d) Litter size among different treatment groups. (e) E14.5 fetal weights for Sham group and PEVs-treated group. (f) E14.5 placental weights for Sham group and PEVs-treated group. Statistical significance was determined by Student's t-test (two-tailed) and one-way analysis of variance (ANOVA) with the Bonferroni post hoc test. ***$P < 0.001$; **$P < 0.01$. The data are presented as mean ± SD.

Use of Laboratory Animals and were approved by the Committee on Ethical Use of Animals of Soochow University (ethical code: SUDA20231012A02).

Use of AI statement

None.

References

[1] Harris, E. Infertility affects 1 in 6 people globally. *JAMA* **2023**, *329*, 1443.

[2] Sbaragli, C.; Morgante, G.; Goracci, A.; Hofkens, T.; De Leo, V.; Castrogiovanni, P. Infertility and psychiatric morbidity. *Fertil. Steril.* **2008**, *90*, 2107–2111.

[3] Pirtea, P.; de Ziegler, D.; Ayoubi, J. M. Uterine infertility, the last frontier. *Fertil. Steril.* **2022**, *118*, 463–464.

[4] de Ziegler, D.; Toner, J. P. Fertility workups: The times they are a-changin'. *Fertil. Steril.* **2022**, *118*, 5–7.

[5] Carbonnel, M.; Pirtea, P.; de Ziegler, D.; Ayoubi, J. M. Uterine factors in recurrent pregnancy losses. *Fertil. Steril.* **2021**, *115*, 538–545.

[6] Khan, Z. Etiology, risk factors, and management of asherman syndrome. *Obstet. Gynecol.* **2023**, *142*, 543–554.

[7] Jin, Z. Q.; Li, J. D.; Yang, E. T.; Shi, H.; Bu, Z. Q.; Niu, W. B.; Wang, F.; Huo, M. Z.; Song, H.; Zhang, Y. L. Effect of endometrial thickness changes on clinical pregnancy rates after progesterone administration in a single frozen-thawed euploid blastocyst transfer cycle using natural cycles with luteal support for PGT-SR- and PGT-M-assisted reproduction: a retrospective cohort study. *Reprod. Biol. Endocrinol.* **2021**, *19*, 154.

[8] Wang, S. M.; Qi, L.; Liu, Y. P.; Shi, H.; Chen, X. L.; Wang, N. N.; Su, Y. C. Suitable endometrial thickness on embryo transfer day may reduce ectopic pregnancy rate and improve clinical pregnancy rate. *BMC Pregnancy Childbirth* **2023**, *23*, 517.

[9] Lv, H. N.; Zhao, G. F.; Jiang, P. P.; Wang, H. Y.; Wang, Z. Y.; Yao, S. M.; Zhou, Z. H.; Wang, L. M.; Liu, D.; Deng, W. B. et al. Deciphering the endometrial niche of human thin endometrium at single-cell resolution. *Proc Natl Acad Sci USA* **2022**, *119*, e2115912119.

[10] Gharibeh, N.; Aghebati-Maleki, L.; Madani, J.; Pourakbari, R.; Yousefi, M.; Ahmadian Heris, J. Cell-based therapy in thin endometrium and Asherman syndrome. *Stem Cell Res. Ther.* **2022**, *13*, 33.

[11] Oneto, P.; Etulain, J. PRP in wound healing applications. *Platelets* **2021**, *32*, 189–199.

[12] Everts, P.; Onishi, K.; Jayaram, P.; Lana, J. F.; Mautner, K. Platelet-rich plasma: New performance understandings and therapeutic considerations in 2020. *Int. J. Mol. Sci.* **2020**, *21*, 7794.

[13] Sharara, F. I.; Lelea, L. L.; Rahman, S.; Klebanoff, J. S.; Moawad, G. N. A narrative review of platelet-rich plasma (PRP) in reproductive medicine. *J. Assist. Reprod. Genet.* **2021**, *38*, 1003–1012.

[14] Dohan Ehrenfest, D. M.; Rasmusson, L.; Albrektsson, T. Classification of platelet concentrates: From pure platelet-rich plasma (P-PRP) to leucocyte- and platelet-rich fibrin (L-PRF). *Trends Biotechnol.* **2009**, *27*, 158–167.

[15] Jurk, K.; Kehrel, B. E. Platelets: Physiology and biochemistry. *Semin. Thromb. Hemost.* **2005**, *31*, 381–392.

[16] Ramaswamy Reddy, S. H.; Reddy, R.; Babu, N. C.; Ashok, G. N. Stem-cell therapy and platelet-rich plasma in regenerative medicines: A review on pros and cons of the technologies. *J. Oral Maxillofac. Pathol.* **2018**, *22*, 367–374.

[17] Everts, P. A.; van Erp, A.; DeSimone, A.; Cohen, D. S.; Gardner, R. D. Platelet rich plasma in orthopedic surgical medicine. *Platelets* **2021**, *32*, 163–174.

[18] Ma, Q. L.; Fan, Q.; Xu, J. L.; Bai, J. Y.; Han, X.; Dong, Z. L.; Zhou, X. Z.; Liu, Z.; Gu, Z.; Wang, C. Calming cytokine storm in pneumonia by targeted delivery of TPCA-1 using platelet-derived extracellular vesicles. *Matter* **2020**, *3*, 287–301.

[19] Zhu, W. D.; Dong, Y. Q.; Xu, P. C.; Pan, Q.; Jia, K. Y.; Jin, P. S.; Zhou, M.; Xu, Y. B.; Guo, R.; Cheng, B. A composite hydrogel containing resveratrol-laden nanoparticles and platelet-derived extracellular vesicles promotes wound healing in diabetic mice. *Acta Biomater.* **2022**, *154*, 212–230.

[20] Dai, Z. Q.; Xia, C.; Zhao, T. X.; Wang, H. L.; Tian, H. S.; Xu, O. Y.; Zhu, X. B.; Zhang, J.; Chen, P. F. Platelet-derived extracellular vesicles ameliorate intervertebral disc degeneration by alleviating mitochondrial dysfunction. *Mater. Today Bio* **2023**, *18*, 100512.

[21] Antich-Rosselló, M.; Forteza-Genestra, M. A.; Monjo, M.; Ramis, J. M. Platelet-derived extracellular vesicles for regenerative medicine. *Int. J. Mol. Sci.* **2021**, *22*, 8580.

[22] Meng, W. R.; He, C. S.; Hao, Y. Y.; Wang, L. L.; Li, L.; Zhu, G. Q. Prospects and challenges of extracellular vesicle-based drug delivery system: Considering cell source. *Drug Deliv.* **2020**, *27*, 585–598.

[23] Vader, P.; Mol, E. A.; Pasterkamp, G.; Schiffelers, R. M. Extracellular vesicles for drug delivery. *Adv. Drug Deliv. Rev.* **2016**, *106*, 148–156.

[24] Zhang, X.; Zhang, H. B.; Gu, J. M.; Zhang, J. Y.; Shi, H.; Qian, H.; Wang, D. Q.; Xu, W. R.; Pan, J. M.; Santos, H. A. Engineered extracellular vesicles for cancer therapy. *Adv. Mater.* **2021**, *33*, 2005709.

[25] Zhou, Z. Y.; Luo, R. F.; Chen, L.; Hu, C.; Chen, C.; Maitz, M. F.; Li, L. H.; Yang, L.; Deng, D.; An, Y. Q. et al. Dressing blood-contacting devices with platelet membrane enables large-scale multifunctional biointerfacing. *Matter* **2022**, *5*, 2334–2351.

[26] Ma, Q. L.; Yao, C. L.; Wu, Y.; Wang, H.; Fan, Q.; Yang, Q. Y.; Xu, J. L.; Dai, H. X.; Zhang, Y.; Xu, F. et al. Neurological disorders after severe pneumonia are associated with translocation of endogenous bacteria from the lung to the brain. *Sci. Adv.* **2023**, *9*, eadi0699.

[27] Cao, Y. M.; Qi, J.; Wang, J.; Chen, L.; Wang, Y.; Long, Y. J.; Li, B. Y.; Lai, J. L.; Yao, Y. J.; Meng, Y. W. et al. Injectable "homing-like" bioactive short-fibers for endometrial repair and efficient live births. *Adv. Sci. (Weinh.)* **2024**, *11*, 2306507.

[28] Lee, D.; Ahn, J.; Koo, H. S.; Kang, Y. J. Intrauterine botulinum toxin A administration promotes endometrial regeneration mediated by IGFBP3-dependent OPN proteolytic cleavage in thin endometrium. *Cell. Mol. Life Sci.* **2023**, *80*, 26.

[29] Yi, X.; Liu, F.; Gao, K. J.; Chen, F.; Wang, Y. F.; Li, H. Y.; Wang, X. F.; Huang, Y.; Fu, H. J.; Zhou, W. J. et al. Reconstructable uterus-derived materials for uterus recovery toward efficient live births. *Adv. Mater.* **2022**, *34*, 2106510.